ISSN 0036-0244, Russian Journal of Physical Chemistry A, 2022, Vol. 96, No. 5, pp. 1051–1061. © Pleiades Publishing, Ltd., 2022.

PHYSICAL CHEMISTRY OF NANOCLUSTERS AND NANOMATERIALS

Nano-metallic Semiconductor towards the Vibrational Analysis and Harmonic Linear Combination

Fatemeh Mollaamin[a,*], Majid Monajjemi[a,b], and Hossein Sakhaeinia[b]

[a] *Department of Biomedical Engineering, Faculty of Engineering and Architecture, Kastamonu University, Kastamonu, Turkey*

[b] *Department of Chemical Engineering, Central Tehran Branch, Islamic Azad University, Tehran, Iran*

** e-mail: smollaamin@gmail.com*

Received May 6, 2021; revised June 1, 2021; accepted June 3, 2021

Abstract—Nanotechnology is presently dealt with development in the process of becoming an indispensable phenomenon in the engineering and scientific fields. In this work, it has been proved that the (8, 0) zig-zag GaN, GaP, GaAs, InN, InP, and InAs nanotubes can act as semiconductors. For historical reasons, normal mode analysis was originally developed for describing the vibrational spectra of molecules. A very useful approach in the analysis of normal modes is to turn attention away from individual modes and towards the types of motion in the nanotube that one would like to analyze. By calculation of the normal modes using the U matrix, it is possible to get the F matrix from the multiplication of frequency to the U matrix. In this work a complete set of the linear combinations and their normalization coefficients are achieved. The fact that for zigzag tubes, the IR-active modes are different in the (8, 0) zig-zag GaN, GaP, GaAs, InN, InP, and InAs nanotubes and is due to the reduced symmetry for those compounds. In this Letter, a simple yet accurate computational frequency normal mode was derived for estimating the nanotubes that are corresponding with some behavior of them.

Keywords: vibration modes, semiconductor nanotubes, symmetry, GaN, GaP, GaAs, InN, InP, InAs

DOI: 10.1134/S0036024422050090

INTRODUCTION

Nanotechnology refers to integration of artificial materials of infinitesimal sizes into large components of devices and structures and has caused life comfortable in a variety of ways through faster and safer devices.

Semiconductor nanowires exhibit a variety of unique material properties, including mechanical flexibility, size-dependent optical and electronic properties, and solution process ability [1–3].

Group III–V nitride semiconductors are getting considerable attention to their applications for solid lighting and optoelectronics such as quantum dots, nano-rods, nanowires and nanotubes have also become interesting subjects because of the wide range of potential applications in short-wavelength optoelectronic devices [4–6].

Boron-nitride (BN) was the first chemical compound to replace elemental carbon in nanotubes because of its hexagonal structure which is similar to graphite [7]. Boron nitride nanotubes were first synthesized in 1995 [8].

Boron nitride also has a wonderful thermal and chemical stability. The thermal conductivity of BN is among the highest of all electric insulators. Moreover, the electronic and electromagnetic behaviors of boron nitride have been known in non-bonded interactions [9–12].

Substitution of the carbon–carbon pairs wholly by the boron–nitrogen pairs in the hexagonal arrangement of graphite leads to the formation of a wide array of two-dimensional segments [13–15].

Aluminum nitride nanotubes have been found to have semiconducting band gaps. The lower strain energy is required in order to wrap up an AlN graphitic sheet into a tube. Contrary to the cases of carbon nanotubes, the band gap of AlN nanotubes rises with the growing diameter of the tubes and inundates at a value consequent to the calculated band gap of an AlN hexagonal sheet [16]. Gallium nitride (GaN) nanotubes were synthesized in 2005 [17].

They have been identified with excellent electronic and optical properties. By ab-initio calculations there have also been shown that the conduction of GaN nanotubes can be modulated by an external transverse electric field [18].

These possibilities may open up new exciting applications within areas such as biochemical sensing, nano-fluidics, and optoelectronics. However, in order to realize these types of new applications, techniques

for synthesis of high quality nanotubes have to be further developed [19–23].

Although the confinement effects on electronic and optical properties of these structures have been investigated, much less is known about their vibrational properties. The phonons from the bulk with their well-studied dispersions collapse into discrete states, or vibrons [24] in the case of 3D confinement given in quantum dots (QDs).

These excitations allow carriers to relax down the discrete ladder of electronic or excited states. For the larger self-assembled quantum dots, the electronic and excited states are believed to enter a strong coupling regime with the phonons to form polarons [25, 26]. They are proposed as explanation for the lack of phonon-bottleneck [27].

In colloidal nano-crystals the reasons for the lack of phonon-bottleneck is still under debate but is likely to involve vibrons [28, 29].

Vibrational properties are also most relevant to the loss of quantum coherence including a process, which limits the application of quantum dots in the field of quantum optics and information science.

The main persuasion of this study is that III–V compound semiconductors are used for the highest-performance optical sources and detectors, and are being used in high-speed and high-frequency digital and analog devices.

THEORETICAL CONCEPTS

The projection operators have been used for finding a function or the displacement pattern of eigenvectors transforming as a particular irreducible representation. For example, the function of F can be expanded into several irreducible representations,

$$F = \sum_{\alpha}\sum_{n} c_{\alpha}^{n}\zeta_{\alpha}^{n} \quad , \tag{1}$$

where α labels the irreducible representations, c_{α}^{n} are the coefficients of the expansion, and the ζ_{α}^{n} are functions transforming according to the representation α. A projection operator defined by

$$P_{l(n)}^{(\beta)} = \frac{d_{\beta}}{g}\sum_{G} D_{ln}^{(\beta)}(G)^{*}(G), \tag{2}$$

applied to F picks out the symmetry adapted function $\zeta_{l}^{(\beta)}$.

In this equation d_{β} is the degeneracy of the irreducible representation β, g the order of the symmetry group, G are the symmetry operations, and $D_{ln}^{(\beta)}$ is the lnth element of the representation matrix $D^{(\beta)}$. From a given function, and its irreducible presentation, functions can be generating if that function has a "component" or a "nonzero projection" along the irreducible presentation of interest. This explains the name of "projector." As an example, if there is an orthonormal set Li of the function $\varnothing_{1}^{i}, \varnothing_{2}^{i}, \varnothing_{\mathrm{Li}}^{i}$, which is used to form the ith irreducible representation of a group by order h, for each operator, **R** in the group, by definition we can have:

$$\hat{\mathbf{R}}\varnothing_{t}^{i} = \sum_{s}\varnothing_{s}^{i}\Gamma(R)_{st}^{i}. \tag{3}$$

By multiply Eq. (3) to $[\Gamma(R)_{s't'}^{i}]^{*}$ and sum all over the symmetrical functions in the group it will be yielded:

$$\sum_{R}[\Gamma(R)_{s't'}^{i}]^{*}\hat{\mathbf{R}}\varnothing_{t}^{i} = \sum_{R}\sum_{s}\varnothing_{s}^{i}\Gamma(R)_{st}^{i}[\Gamma(R)_{s't'}^{i}]^{*}. \tag{4}$$

Considering $\varnothing_{s}^{i}$ are functions independent from R, the right side of Eq. (4) can be written as:

$$\sum_{s}\varnothing_{s}^{i}\sum_{R}\Gamma(R)_{st}^{i}[\Gamma(R)_{s't'}^{i}]^{*}. \tag{5}$$

Therefore, we have a series of Li terms and each of them is equal to a production of $\varnothing_{s}^{i}$ and a coefficient. These coefficients are following the orthogonality rule:

$$\sum_{R}\Gamma(R)_{st}^{i}[\Gamma(R)_{s't'}^{i}]^{*} = h/(L_{i}L_{j})^{1/2}\delta_{ij}\delta_{ss'}\delta_{tt'}. \tag{6}$$

By use of Eqs. (6), (4) is simplified as follows:

$$\sum_{R}[\Gamma(R)_{st}^{i}]^{*}\mathbf{R}\varnothing_{t}^{i} = \left(\frac{h}{L_{j}}\right)\varnothing_{s'}^{i}\delta_{ij}\delta_{tt'}. \tag{7}$$

Now, by introducing

$$\mathbf{P}_{s't'}^{j} = \frac{L_{j}}{h}\Gamma(R)_{st}^{i}[\Gamma(R)_{s't'}^{i}]^{*}\mathbf{R}. \tag{8}$$

Equation (7) gives:

$$\mathbf{P}_{s't'}^{j}\varnothing_{t}^{i} = \varnothing_{s'}^{i}\delta_{ij}\delta_{tt'}, \tag{9}$$

which $\mathbf{P}_{s't'}^{j}$ is projection operator.

The application of this operator on each $\varnothing_{t}^{i}$ is nonzero only when this function or some of its terms is a function of $\varnothing_{s'}^{i}$. One of the most important applications of this operator is projecting function $\varnothing_{t}^{i}$ from any function $\varnothing_{t}^{i}$.

In other words

$$\mathbf{P}_{t''t'}^{j}\varnothing_{t}^{i} = \varnothing_{t'}^{i}\delta_{ij}\delta_{tt'}. \tag{10}$$

By use of the projection operator on the base of L_{j} diagonal elements of a matrix, some $\varnothing_{t}^{i}$ functions have been yielded, which are the bases for the jth irreducible presentation [30].

Table 1. Optimized parameters of total energy, binding energy, isolated atomic energy, electronic energy, core–core interaction and heat of formation (kcal/mol) for GaN, GaP, GaAs, InN, InP, and InAs nanotubes

Nanotube	Total energy	Binding energy	Isolated atomic energy	Electronic energy	Core–core interaction	Heat of formation
GaN	140586.30	259548.96	–118962.66	–1262468.33	1403054.63	263830.56
GaP	182111.58	279126.63	–97015.04	–1158335.93	1340447.52	282509.91
GaAs	192149.76	291751.69	–99601.93	–1171913.62	1364063.38	295056.49
InN	145693.66	261693.62	–115999.96	–1235159.69	1380853.35	265797.62
InP	134150.44	228202.79	–94052.35	–1184048.49	1318198.93	231408.47
InAs	143839.13	240478.37	–96639.24	–1197581.33	1341420.46	243605.57

By assuming $\Gamma_k(p)_{ij}$ as the ijth element of the matrix, the pth operator ($\mathbf{O}_p$) in the kth irreducible presentation can be shown. By this assumption the operator $\mathbf{O}_{k,ij}$ is defined as follows

$$\mathbf{O}_{k,ij} = L_k/h\sum_p\sum_k (p)^*_{ij}\mathbf{O}_p, \quad (11)$$

where h is group order and L_k is the presentation dimension.

By $i = j$ these operators called "projection operators" ($\mathbf{P}_{k,ii}$):

$$\mathbf{P}_{k,ii} = \mathbf{O}_{k,ii}. \quad (12)$$

By $i \neq j$. The non-diagonalized operators are called Transfer operators or shift operators,

$$\mathbf{T}_{k,ij} = \mathbf{O}_{k,ij}. \quad (13)$$

In one-dimensional presentations $\mathbf{P}_{k,ij}$ and $\mathbf{O}_{k,ii}$ are the same and there is no $\mathbf{T}_{k,ij}$. With use of the above definitions, making the irreducible basis becomes possible in the following way. At first, the point group of the molecule is determined. Then the character of the system (Γ_{angles} or Γ_{bonding}) is calculated.

By using the standard reduces, formulation of these characters can be reduced to give the irreducible representations:

$$n_\Gamma = \frac{1}{h}\sum_g n_g\chi_R\chi_\Gamma, \quad (14)$$

where n_g is the number of the symmetry operation in the class of g, χ_R is the character of reducible presentation and χ_Γ is the character of irreducible presentation for the symmetric operations of class g. In the part there is a note about the reducing the $C \infty v$ and $D \infty h$ point groups [31–37].

At the next step, the interested function is written by use of the projection operator. A set of the results gives the internal coordinate system for a given point group. There are several examples to illustrate this procedure in Table 1. With use of the resulting coordinate system, the U matrix (UMAT) can be written easily. These are matrices, which perform the linear transformations on the internal coordinate's sets [38].

RESULTS AND DISCUSSION

Electronic structure calculations have been successful in portending and illustrating the properties of materials. Pseudo potentials provide a further simplification, since they delete the need to explicitly consider the core electrons.

Designing of Theoretical Model

The (8, 0) zig-zag GaAs, GaN, and GaP nanotube semiconductors with C_{6v} show a much higher IR absorbance than C nanotubes (Fig. 1) [39–41].

It is expected that the IR spectroscopy will develop into a standard characterization tool for GaN, GaP, GaAs, InN, InP, and InAs nanotubes such as it is already in the case of C tubes. It is very significant to have a detailed knowledge of phonon frequencies in GaN, GaP, GaAs, InN, InP, and InAs nanotubes and to understand the dependence on diameter and chirality, in order to guide future experiments.

In IR spectroscopy, only phonons at (or close to) the Γ point of the one-dimensional Brillouin zone can be excited (as long as we restrict our discussion to first-order processes).

Energy minima of GaN, GaP, GaAs, InN, InP, and InAs nanotubes were carried out by semi empirical method for optimizing the structure of the nanotube. All the normal mode frequencies and IR intensity were calculated using the optimized structure [42, 43].

Semi-Empirical Method

The cost of performing an HF calculation scales formally as the fourth power of the number of basic functions. This arises from the number of semi-empir-

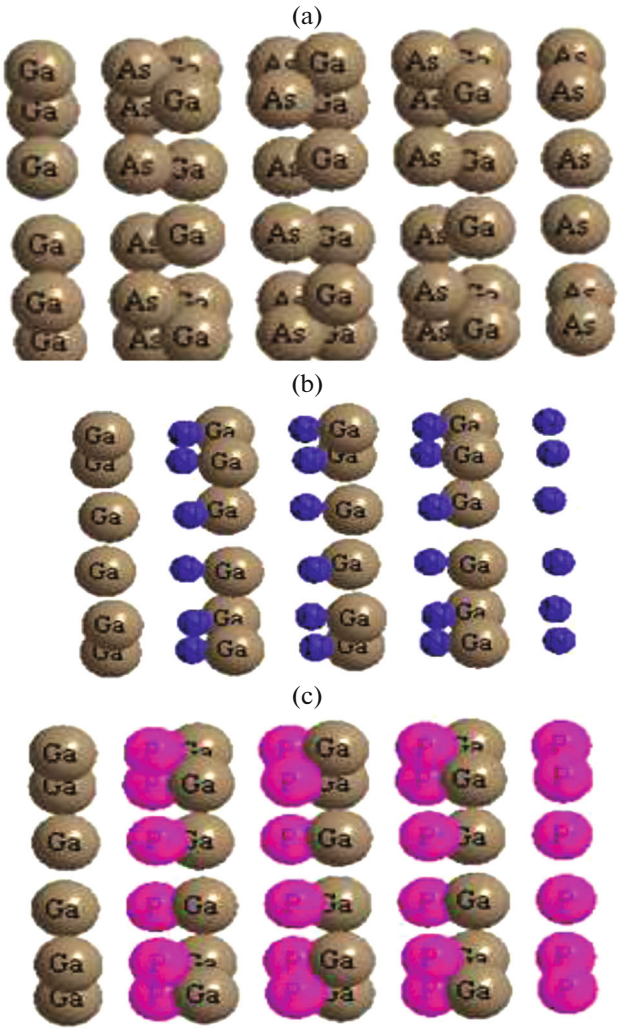

Fig. 1. The (8, 0) zig-zag GaAs, GaN, and GaP nanotube semiconductors with C_{6v} point group.

ical methods reduce the computational cost by reducing the two-electron integrals necessary for constructing the Fock matrix [44].

The core–core repulsion is the repulsion between nuclear charges, properly reduced by the number of core electrons. the core-core repulsion of the modified neglect of diatomic overlap (mndo) model has given in [45].

The core–core function was also modified by adding Gaussian functions, and the whole model was re-parameterized [46].

The electronic properties of GaN, GaP, GaAs, InN, InP, and InAs semiconductors were investigated known. So from theoretical calculations it has been shown that the band gap depends on composition.

In this study, the relation between size and electronic band structure of the GaN, GaP, GaAs, InN, InP, and InAs nanotubes observed in detail (Table 1).

All atomic positions and lattice parameters are optimized by using the semi empirical calculations where total energy and atomic forces are minimized. It has been exhibited that for a structure with a larger atomic radius, the conduction band minimum increases differently at GaN, GaP, GaAs, InN, InP, and InAs nanotubes (Fig. 2).

In this work, these semiconductor nanotubes have been modeled by using the semi empirical method. Certain discrepancies have been reported in the transition region of the IV characteristics of the semiconductor nanotubes.The design was proposed with optimized parameters such as total energy, binding energy, isolated atomic energy, electronic energy, core–core interaction and heat of formation for GaN, GaP, GaAs, InN, InP, and InAs nanotubes (Table 1).

By comparison of semi empirical calculation for GaN, GaP, GaAs, InN, InP, and InAs nanotubes (8, 0) with C_{6v} point group in Fig. 3, we have found the best relation coefficients of $R^2 = 0.9799$ (total energy), $R^2 = 0.9726$ (electronic energy), $R^2 = 0.9873$ (core–core interaction) and $R^2 = 0.9782$ (heat of formation).

Applying the Primitive's Harmonic Vibrations and UMAT Procedure

Vibrational properties are also most relevant to the loss of quantum coherence; a process, which limits the application of quantum, dots in the field of quantum optics and information science.

In order to calculate vibrons for high quality nanostructures, one must be able to address diameters ranging from several to tens of nanometers. Indeed, smaller structures tend to exhibit poor optical characteristics and show large variations within one sample.

The derivation of an empirical potential for the calculation of vibrons is the ability to use the potential to the structure. This is persuaded by the point that a compound will be entitled to the existence of different frequencies.

So, a complete set of the linear combinations and their normalization coefficients are accomplished. The irreducible representations of the symmetry group have been shown by A and B (Table 2). We have applied the usage of projection operator method in finding the coordinate system, and by using it the U matrix is written and finally the frequencies and distributions of peak position have been gained. The (8, 0) zig-zag GaN, GaP, GaAs, InN, InP, and InAs semiconductor nanotubes with possible applications in the realm of nanostructures and 138 normal modes

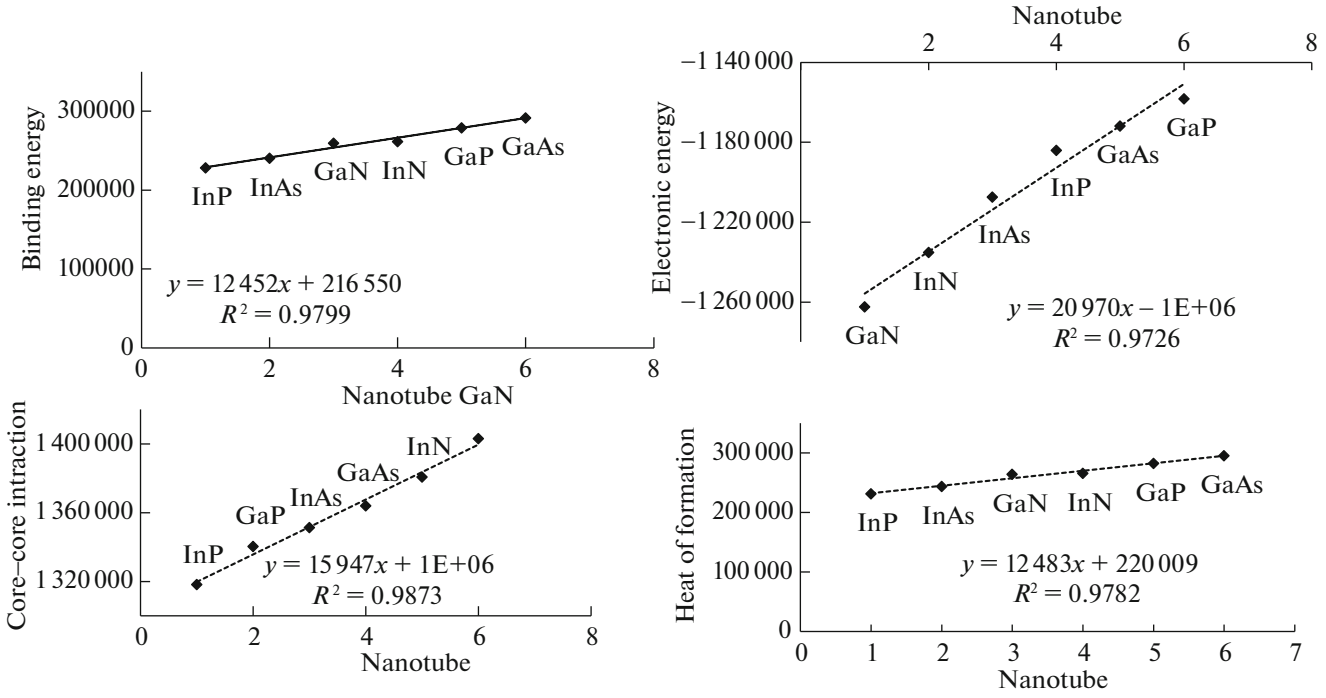

Fig. 2. Optimized parameters of total energy, binding energy, isolated atomic energy, electronic energy, core–core interaction and heat of formation (kcal/mol) for the GaN, GaP, GaAs, InN, InP, and InAs nanotubes.

were probed. The character of the system assigned by Γ was achieved from the character tables. Vibrational calculation was calculated by the MOLVIB algorithms and by Hyper Chem [47].

Survey of Normal Mode Analysis of Infrared Spectroscopy and Group Theory

Normal mode analysis is one of the standard techniques in the study of the dynamics of nanotubes. It is primarily applied for identifying and characterizing the slowest motions in a poly system, which are inaccessible by other methods. This text explains what normal mode analysis is and what one can do with it without going beyond its limit of validity.

By definition, normal mode analysis is the study of harmonic potential wells by analytic means. The first section of this study has been dealt with potential wells and harmonic approximations. This work is about normal mode methods to different physical situations, and it is discusses how useful information can be accomplished from normal modes.

Normal mode coordinates are achieved by a linear combination of Cartesian coordinates. They include simultaneous motion of all atoms during the vibration, which leads to a natural description of molecular vibrations. Therefore, they are good candidates for representation of the molecular Hamiltonian.

Since a transformation between different sets of coordinates is possible, the non-harmonic terms can be calculated in one representation, and then transformed into another one.

For systems with translational symmetry, the "point group in the space group" determines through the selection rules which modes are active or inactive [48, 49].

The unit cell of a (n, 0) zigzag tube possesses an n-fold rotation axis. In addition, n (even $2n$) vertical reflection-symmetry planes can be found. So, the unit cell of a zigzag tube transforms under the C_{nv} symmetry group. In the infinitely extended tube, the operations of the C_{nv} point group are valid as well, but in addition, a rotation by $\Phi/2$ with subsequent translation by $T/2$ also maps the system onto itself. This leads to the conclusion that for the infinitely extended system, the C_{2nv} symmetry group is the relevant one for symmetry analysis of IR-active modes.

Analogously, for (n, m) armchair tubes, the symmetry group of the unit cell is C_{nh} and the symmetry group of the infinitely extended tube is $C_{2nh.}$ Finally, for chiral (n, m) tubes, the unit cell has the low point-group symmetry C_d, where d is the greatest common divisor of n and m. However, the infinitely extended tube is described by the C_N symmetry group, where N is the number of hexagons (=2 times the number of atoms) per unit cell which is, in general, much larger than d. The number of active modes is found by

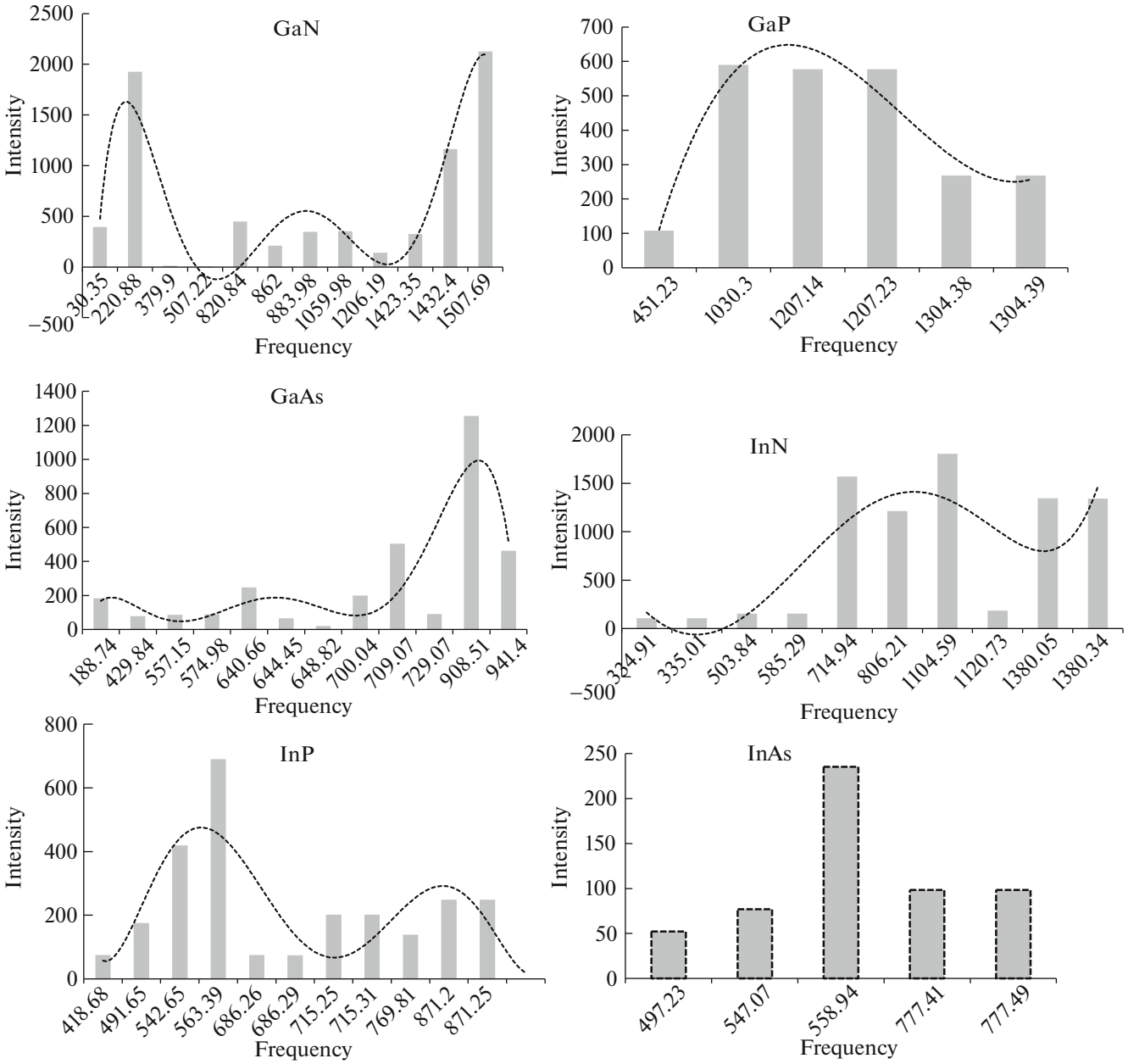

Fig. 3. The natural logarithms frequency (cm^{-1}) and intensity (km/mol) of some different media of water and methanol and water-methanol mixed versus normal mode for BN zigzag tube (8, 0) with C_{6v} point group by AM1 calculation.

determining how often each irreducible representation appears in the (reducible) representation of the symmetry group (C_{2nv}, C_{2nh}, or C_N, respectively) which is given by the $12n$ vibration degrees of freedom of the unit cell. For zigzag tubes this leads to 8 IR modes (3 with A1 symmetry, 5 with E1 symmetry) are active [49].

Under certain experimental conditions, if the tubes are short compared to the wavelength of the scattered laser light, the tubes are expected to display the spectroscopic properties of very large molecules rather than of infinitely extended systems (finite-size effect).

In this paper we have also exhibited the main results of the frequencies and intensities of active modes in the (8, 0) zig-zag GaN, GaP, GaAs, InN, InP, and InAs semiconductor nanotubes (Table 3).The normal modes of BNNT can usually be associated with a certain kind of motion of the molecule (Fig. 3).

Nevertheless, it is clear that this simple model captures the main frequency of the spectra, giving support

Table 2. The irreducible representations of the symmetry group have been shown by A and B for the (8, 0) zig-zag GaN, GaP, GaAs, InN, InP, and InAs nanotube semiconductors with C_{6v} point group

C_{2v}	E C$_2$ σv σv	Primitive	Reduced presentation	Linear combination of primitives based on their symmetric A2 A2 B2 B2
Γ1	3 1 1 3	3	2A1 B2	S1(A1) = 1/√2(R1+R2), S2(B2) = 1/√2(R1−R2), S3(A1) = R3
Γ2	3 1 1 3	3	2A1 B2	S4(A1) = 1/√2(R4+R5), S5(B2) = 1/√2(R4−R5), S6(A1) = R6
Γ3	3 1 1 3	3	2A1 B2	S7(A1) = 1/√2(R7+R8), S8(B2) = (R7−R8), S9(A1) = R9
Γ4	3 1 1 3	3	2A1 B2	S10(A1) = 1/√2(R10+R11), S11(B2) = (R10−R11), S12(A1) = R12
Γ5	3 1 1 3	3	2A1 B2	S13(A1) = 1/√2(R13+R14), S14(B2) = 1/√2(R13−R14), S15(A1) = R15
Γ6	3 1 1 3	3	2A1 B2	S16(A1) = 1/√2(R16+R17), S17(B2) = 1/√2(R16−R17), S18(A1) = R18
Γ7	3 1 1 3	3	2A1 B2	S19(A1) = 1/√2(R19+R20), S20(B2) = 1/√2(R19−R20), S21(A1) = R21
Γ8	3 1 1 3	3	2A1 B2	S22(A1) = 1/√2(R22+R23), S23(B2) = 1/√2(R22−R23), S24(A1) = R24
Γ9	3 1 1 3	3	2A1 B2	S25(A1) = 1/√2(R25+R26), S26(B2) = 1/√2(R25−R26), S27(A1) = R27
Γ10	3 1 1 3	3	2A1 B2	S28(A1) = 1/√2(R28+R29), S29(B2) = 1/√2(R28−R29), S30(A1) = R30
Γ11	3 1 1 3	3	2A1 B2	S31(A1) = 1/√2(R31+R32), S32(B2) = 1/√2(R31−R32), S33(A1) = R33
Γ12	3 1 1 3	3	2A1 B2	S34(A1) = 1/√2(R34+R35), S35(B2) = 1/√2(R34−R35), S36(A1) = R36
Γ13	12 2 2 2	5A1 2A2 2B1 3B2	12	S37(A1) = 1/2(R37+R38+R39+R2), S38(A2) = 1/2(R37−R38+R39−R2), S39(B1) = 1/2(−R37−R38+R39+R2), S40(A1) = 1/√2(R40+R41), S41(B2) = 1/√2(R40−R41), S42(A1) = 1/√2(R42+R43), S43(B2) = 1/√2(R42−R43), S44(A1) = 1/2(R44+R45+R46+R47), S45(B1) = 1/2(R44−R45+R46−R47), S46(A2) = 1/2(R44−R45−R46+R47), S47(A1) = 1/√2(R48+R49), S48(B2) = 1/√2(R48−R49),
Γ14	12 2 2 2	5A1 2A2 2B1 3B2	12	S49(A1) = 1/2(R50+R51+R52+R8), S50(A2) = 1/2(R50−R51+R52−R8), S51(B1) = 1/2(−R50−R51+R52+R8), S52(A1) = 1/√2(R41+R53), S53(B2) = 1/√2(R41−R53), S54(A1) = 1/√2(R54+R55), S55(B2) = 1/√2 (R54−R55), S56(A1) = 1/2(R56+R57+R58+R59), S57(B1) = 1/2(R56−R57+R58−R59), S58(A2) = 1/2(R56−R57−R58+R59), S59(A1) = 1/√2(R60+R61), S60(B2) = 1/√2(R60−R61)
Γ15	12 2 2 2	5A1 2A2 2B1 3B2	12	S61(A1) = 1/2(R62+R63+R11+R64), S62(A2) = 1/2(R62−R63+R11−R64), S63(B1) = 1/2(−R62−R63+R11+R64), S64(A1) = 1/√2(R65+R66), S65(B2) = 1/√2(R65−R66), S66(A1) = 1/√2(R67+R68), S67(B2) = 1/√2(R67−R68), R68(A1) = 1/2(R69+R70+R71+R72), R69(B1) = 1/2(R69−R70+R71−R72), S70(A2) = 1/2(R69−R70−R71+R72), S71(A1) = 1/√2(R61+R73), S72(B2) = 1/√2(R61−R73)

Table 2. (Contd.)

C_{2v}	E C_2 σv σv	Primitive	Reduced presentation	Linear combination of primitives based on their symmetric A2 A2 B2 B2
Γ16	12 2 2 2	5A1 2A2 2B1 3B2	12	S73(A1) = 1/2(R74+R63+R75+R17), S74(A2) = 1/2(R74–R63+R75–R17), S75(B1) = 1/2(–R74–663+R75+R17), S76(A1) = 1/√2(R76+R77), S77(B2) = 1/√2(R76–R77), S78(A1) = 1/√2(R78+R79), S79(B2) = 1/√2(R78–R79), S80(A1) = 1/2(R80+R81+R82+R83), S81(B1) = 1/2(R80–R81+R82–R83), S82(A2) = 1/2(R80–R81–R82+R83), S83(A1) = 1/√2(R84+R85), S84(B2) = 1/√2(R84–R85)
Γ17	12 2 2 2	5A1 2A2 2B1 3B2	12	S85(A1) = 1/2(R86+R19+R37+R87), S86(A2) = 1/2(R86–R19+R37–R87), S87(B1) = 1/2(–R86–R19+R37+R87), S88(A1) = 1/√2(R90+R91), S89(B2) = 1/√2(R90–R91), S90(A1) = 1/√2(R88+R89), S91(B2) = 1/√2(R88–R89), S92(A1) = 1/2(R92+R93+R94+R95), S93(B1) = 1/2(R92–R93+R94–R95), S94(A2) = 1/2(R92–R93–R94+R95), S95(A1) = 1/√2(R96+R97), S96(B2) = 1/√2(R96–R97)
Γ18	12 2 2 2	5A1 2A2 2B1 3B2	12	S97(A1) = 1/2(R25+R98+R62+R99), S98(A2) = 1/2(R25–R98+R62–R99), S99(B1) = 1/2(–R25–R98+R62+R99), S100(A1) = 1/√2(R91+R100), S101(B2) = 1/√2(R91–R100), S102(A1) = 1/√2(R101+R102), S103(B2) = 1/√2(R101–R102), S104(A1) = 1/2(R103+R104+R105+R106) S105(B1) = 1/2(R103–R104+R105–R106), S106(A2) = 1/2(R103–R104–R105+R106), S107(A1) = 1/√2(R107+R108), S108(B2) = 1/√2(R107–R108)
Γ19	12 2 2 2	5A1 2A2 2B1 3B2	12	S109(A1) = 1/2(R109+R28+R110+R51), S110(A2) = 1/2(R109–R28+R110–R51), S111(B1) = 1/2(–R109–R28+R110+R51), S112(A1) = 1/√2(R111+R112), S113(B2) = 1/√2(R111–R112), S114(A1) = 1/√2(R113+R114) S115(B2) = 1/√2(R113–R114), S116(A1) = 1/2(R115+R116+R117+R118), S117(B1) = 1/2(R115–R116+R117–R118), S118(A2) = 1/2(R115–R116–R117+R118), S119(A1) = 1/√2(R119+R120), S120(B2) = 1/√2(R119–R120)
Γ20	12 2 2 2	5A1 2A2 2B1 3B2	12	S121(A1) = 1/2(R34+R121+R74+R122), S122(A2) = 1/2(R34–R121+R74–R122), S123(B1) = 1/2(–R34–R121+R74+R122), S124(A1) = 1/√2(R123+R112), S125(B2) = 1/√2(R123–R112), S126(A1) = 1/√2(R124+R125), S127(B2) = 1/√2(R124–R125), S128(A1) = 1/2(R126+R127+R128+R129), S129(B1) = 1/2(R126–R127+R128–R129), S130(A2) = 1/2(R126–R127–R128+R129), S131(A1) = 1/√2(R130+R131), S132(B2) = 1/√2(R130–R131)

to the structural model and parameters. Knowing the normal modes thus permits the explicit evaluation of all possible vibrational frequencies in a system.

Vibrational normal mode analysis thus classifies all possible motions around a stable equilibrium state by vibrational frequency. Note that since the range of atomic masses is much smaller than the range of eigenvalues, the difference between energetic and vibrational analysis is not very large (Fig. 3).

Low-frequency modes are therefore to a very good approximation also low-energy modes, and vice versa. It should also be noted that at the high frequency end, quantum effects become important. However, the transformation to normal mode coordinates remains valid in a quantum description; only the dynamic interpretation must be adapted.

CONCLUSIONS

Electronic properties study of nanostructure represents one of the most vibrant fields of condensed matter physics. We derived vibration modes of some molecules by comparison the spectroscopy of optimized force field for GaN, GaP, GaAs, InN, InP, and InAs semiconductors.

Using the group theory and the state of projection operators, a systematic method for getting the vibration model of the zigzag single-walled GaN, GaP, GaAs, InN, InP, and InAs nanotubes with (8, 0) structure was illustrated.

Table 3. Optimized parameters of degeneracy, symmetry, frequency (cm^{-1}) and intensity (km/mol) using semi empirical method for the (8, 0) zig-zag GaN, GaP, GaAs, InN, InP, and InAs nanotube semiconductors with C_{6v} point group

Spectro-scopy	GaN			GaP			GaAs			InN			InP			InAs		
	N	D S	F I	N	D S	F I	N	D S	F I	N	D S	F I	N	D S	F I	N	D S	F I
IR	80	1 E1	30.35 394.12	79	1 E1	451.23 107.68	75	1 E1	188.74 183.75	94	2 E1	334.91 106.62	99	2 B1	418.61 74.49	99	1 A1	497.23 52.10
	81	1 E1	220.88 1925.25	110	1 E1	1030.30 590.17	81	1 E1	429.84 78.70	95	2 E1	335.01 106.61	100	2 B2	418.68 74.59	106	1 A1	547.07 76.90
	83	2 E1	379.90 12.41	128	2 B1	1207.14 577.24	84	1 E1	557.15 87.13	101	2 E1	503.84 154.10	101	1 A1	491.65 175.16	107	1 A1	558.94 235.23
	84	1 E1	507.22 5.71	129	2 B2	1207.23 577.44	86	1 E1	574.98 89.77	102	2 E1	585.29 153.63	106	1 A1	542.65 419.30	134	2 B2	777.41 98.39
	93	1 E1	820.84 449.31	135	1 E1	1304.38 267.77	88	2 E1	640.66 247.85	107	1 E1	714.94 1569.65	107	1 A1	563.39 689.91	135	2 B1	777.49 98.48
	94	1 E1	862.00 209.54	136	1 E1	1304.39 267.80	89	2 E1	644.45 65.38	112	1 E1	806.21 1214.34	116	2 B1	686.26 75.16			
	95	1 E1	883.98 347.90				90	1 E1	648.82 20.49	121	2 E1	1104.59 1805.57	117	2 B2	686.29 74.17			
	96	1 E1	1059.71 351.43				91	1 E1	700.04 199.07	122	2 E1	1120.73 183.65	119	4 B2	715.25 202.01			
	98	1 E1	1206.19 139.37				93	1 E1	709.07 504.63	131	2 E1	1380.05 1344.97	120	4 B1	715.31 202.26			
	106	1 E1	1423.35 325.67				94	1 E1	729.07 91.95	132	2 E1	1380.34 1343.81	124	2 E1	769.81 139.12			
	108	2 E1	1432.40 1162.73				100	1 E1	908.51 1255.63				133	2 E1	871.20 248.97			
	111	1 E1	1507.69 2125.60				103	1 E1	941.40 463.41				134	2 E1	871.25 249.19			
Raman	82	2 E1	370.81 36.72	85	2 E1	552.56 19.87	71	2 E1	67.35 7.03	85	2 E1	118.96 35.44	89	2 E1	110.17 15.39	94	2 B2	308.78 1.97
	85	1 E1	547.58 95.54	86	2 E1	552.73 20.06	72	2 E1	86.34 32.07	86	2 E1	119.12 34.96	90	2 E1	110.19 15.40	100	2 B1	505.73 7.11
	86	1 E1	602.85 42.79	90	2 B1	600.40 50.48	73	1 E1	107.40 49.72	93	1 E1	311.98 44.01	93	2 B1	221.53 15.74	101	2 B2	505.79 7.15
	87	1 E1	618.54 68.46	91	2 B2	600.41 50.59	76	1 E1	203.17 97.81	96	2 E1	545.94 8.27	94	2 B2	221.58 15.79	102	2 B1	521.61 1.50
	88	1 E1	662.60 17.49	95	1 A1	695.24 75.81	77	1 E1	244.61 92.65	97	2 E1	546.07 8.19	95	1 A1	324.73 25.99	103	2 B2	521.72 1.50
	89	1 E1	681.84 33.40	97	1 A1	845.82 52.28	79	1 E1	412.89 22.79	109	2 E1	761.83 5.30	102	2 B1	497.81 50.06	109	2 B1	595.66 6.67
	90	1 E1	705.85 29.31	111	1 A1	1052.92 61.69	80	1 E1	417.17 41.05	113	2 E1	903.21 26.83	103	2 B2	534.76 49.93	110	2 B2	595.73 6.64
	91	1 E1	751.50 19.31				82	1 E1	508.58 41.84	114	2 E1	903.30 26.91	105	2 A1	540.63 0.14	117	2 E1	639.17 1.04
	92	1 E1	793.95 35.58				87	1 E1	622.04 54.92	116	2 E1	985.12 24.52	114	2 B1	668.18 22.35	118	2 E1	639.24 1.06
							96	1 E1	747.36 28.09	117	2 E1	985.28 23.98	115	2 B2	668.22 22.87	121	2 E1	656.67 4.27

Table 3. (Contd.)

Spectro-scopy	GaN			GaP			GaAs			InN			InP			InAs		
	N	D S	F I	N	D S	F I	N	D S	F I	N	D S	F I	N	D S	F I	N	D S	F I
Non-active optical mode	84	1 E1	507.22 0.00	112	2 A2	1055.93 0.00	78	1 E1	314.3 10.11	87	1 E1	164.44 0.00	86	2 E1	69.84 0.00	82	1 B2	34.49 0.00
	100	1 E1	1320.21 0.00	113	2 A1	1055.94 0.00	83	1 E1	527.67 0.61	88	2 E1	204.62 0.00	87	2 E1	69.85 0.00	83	2 A1	91.06 0.00
	123	2 E1	1700.43 0.00	114	1 B1	1099.05 0.00	85	1 E1	564.25 7.43	89	2 E1	204.63 0.00	88	1 E1	105.64 0.00	84	2 A2	91.09 0.00
				115	1 A2	1109.39 0.00	92	1 E1	703.33 9.15	90	1 E1	274.97 0.00	91	2 A2	177.32 0.00	85	1 B1	193.68 0.00
				128	1 B2	1188.39 0.00	98	1 E1	811.28 8.61	91	2 E1	296.61 0.00	92	2 A1	177.50 0.00	86	4 A1	221.75 0.00
				130	1 A2	1228.47 0.00	99	1 E1	824.01 1.81	92	2 E1	296.64 0.00	96	1 B2	360.04 0.00	87	4 A2	221.77 0.00
				131	2 A2	1250.40 0.00	118	2 E1	1042.19 3.90	98	3 E1	564.81 0.00	97	2 A1	399.29 0.00	90	1 B1	267.69 0.00
				132	2 A1	1250.42 0.00	121	2 E1	1053.46 6.34	100	3 E1	566.50 0.00	98	2 A2	399.37 0.00	91	2 A2	295.43 0.00
				133	2 B1	1278.30 0.00	125	2 E1	1070.80 1.62	104	2 E1	615.27 0.00	104	2 A2	540.62 0.00	92	2 A1	295.55 0.00
				134	2 B2	1280.78 0.00				105	1 E1	659.42 0.00	108	2 A2	578.63 0.00	96	1 B2	448.46 0.00

Designations: N—normal mode, D—degeneracy, S—symmetry, F—frequency, and I—intensity.

We exhibited the vibrations in these nanotubes by the calculation and combination via their normalization coefficients of (8, 0) nanotube in C_{6v} point group. The access of the semi empirical potential for the vibrons is the capability to apply the potential to GaN, GaP, GaAs, InN, InP, and InAs semiconductors.

This is motivated that a compound will be right to the existence of different frequencies. Vibrational normal mode analysis justifies all possible motions around a stable equilibrium state by vibrational frequency.

CONFLICT OF INTEREST

The authors declare that they have no conflicts of interest.

REFERENCES

1. E. I. Meletis, C. Politis, and W. Schommers, Quantum Matter **3**, 287 (2014).
2. H. Yilmaz, B. R. Weiner, and G. Morell, Phys. Rev. B **81**, 041312 (2010).
3. P. D. Sia, Rev. Theor. Sci. **2**, 146 (2014).
4. D. Govindharaj, S. Nachimuthu, D. F. Gonsalves, et al., Biointerface Res. Appl. Chem. **10**, 6865 (2020).
5. F. Mollaamin, M. Monajjemi, S. Salemi, and M. T. Baei, Fullerenes Nanotubes Carbon Nanostruct. **19**, 182 (2011).
6. S. K. Gopinath, M. Pari, A. M. Rudrannagari, et al., Biointerface Res. Appl. Chem. **11**, 11390 (2012).
7. N. G. Chopra, R. J. Luyken, K. Cherrey, et al., Science (Washington, DC, U. S.) **269**, 966 (1995).
8. N. G. Chopra, R. J. Luyken, K. Cherrey, et al., Science (Washington, DC, U. S.) **269** (5226), 966 (1995).
9. M. Monajjemi, L. Mahdavian, F. Mollaamin, and M. Khaleghian, Russ. J. Inorg. Chem. **254**, 1465 (2009).
10. M. Khaleghian, M. Zahmatkesh, F. Mollaamin, and M. Monajjemi, Fullerenes Nanotubes Carbon Nanostruct. **19** (4) (2011).
11. M. Monajjemi, M. T. Baie, and F. Mollaamin, Russ. Chem. Bull. **59**, 886 (2010).
12. V. S. Lee, P. Nimmanpipug, F. Mollaamin, et al., Russ. J. Phys. Chem A **283**, 2288 (2009).
13. K. Bakhshi, F. Mollaamin, and M. Monajjemi, J. Comput. Theor. Nanosci. **8**, 763 (2011).
14. M. Monajjemi, F. Mollaamin, M. R. Gholami, et al., Maing Group Met. Chem. **26**, 349 (2003).
15. M. Monajjemi, N. Farahani, and F. Mollaamin, Phys. Chem. Liq. **50**, 161 (2012).
16. A. E. S. Fouda and E. A. Haleem, Biointerface Res. Appl. Chem. **10**, 7023 (2020).

17. P. Deb, H. Kim, V. Rawat, et al., Nano Lett. **5**, 1847 (2005).
18. H. Yilmaz, B. R. Weiner, and G. Morell, Phys. Rev. B **81**, 041312 (2010).
19. M. Monajjemi, S. Afsharnezhad, M. R. Jaafari, et al., Chemistry **17**, 1 (2008).
20. B. Ghalandari, M. Monajjemi, and F. Mollaamin, J. Comput. Theor. Nanosci. **8**, 1212 (2011).
21. E. M. Sarasia, S. Afsharnezhad, B. Honarparvar, et al., Phys. Chem. Liq. **49**, 561 (2011).
22. A. Tahan, F. Mollaamin, and M. Monajjemi, Russ. J. Phys. Chem. A **83**, 587 (2009).
23. M. Monajjemi, M. Noei, and F. Mollaamin, Nucleosides, Nucleotides Nucl. Acids **29**, 9 (2010).
24. C. Trallero-Giner, A. Debernardi, M. Cardona, E. Menendez-Proupin, and A. I. Ekimov, Phys. Rev. B **57**, 4664 (1998).
25. S. Hameau, Y. Guldner, O. Verzelen, et al., Phys. Rev. Lett. **83**, 4152 (1999).
26. O. Verzelen, R. Ferreira, and G. Bastard, Phys. Rev. Lett. **88**, 146803 (2002).
27. U. Bockelmann and G. Bastard, Phys. Rev. B **42**, 8947 (1990).
28. M. Sailaja, D. Sarangi, P. Mohapatra, and B. B. Nanda, Biointerface Res. Appl. Chem. **10**, 5259 (2020).
29. T. Owoyokun, C. M. P. Berumen, A. M. Luévanos, et al., Biointerface Res. Appl. Chem. **11**, 11797 (2021).
30. E. B. Wilson, Jr., J. C. Decius, and P. C. Cross, *Molecular Vibrations; The Theory of Infrared and Raman Vibrational Spectra* (McGraw-Hill, New York, 1955).
31. F. Albert, *Chemical Application of Group Theory* (Wiley-Interscience, New York, 1971).
32. L. Schafer and S. J. Cyvrin, J. Chem. Ed. **48**, 295 (1971).
33. D. P. Strommen and E. P. Lippincott, J. Chem. Ed. **48**, 295 (1971).
34. H. P. Fritzer, Match **3**, 21 (1977).
35. J. M. Alvarino, J. Chem. Ed. **55**, 307 (1978).
36. R. L. Flurry, Jr., J. Chem. Ed. **55**, 638 (1979).
37. D. P. Strommen, J. Chem. Ed. **56**, 640 (1979).
38. J. M. Alvarino and A. Chammoro, J. Chem. Ed. **57**, 785 (1980).
39. E. T. Mickelson, C. B. Huffman, A. G. Rinzler, et al., Chem. Phys. Lett. **296**, 188 (1998).
40. P. Driva, M. Sapka, A. Karatzas, et al., Biointerface Res. Appl. Chem. **10**, 4764 (2020).
41. S. Olszewski, Rev. Theor. Sci. **1**, 344 (2013).
42. S. Mondal, M. K. Siddiqui, N. De, and A. Pa, Biointerface Res. Appl. Chem. **11**, 9372 (2021).
43. S. Celasun, Rev. Theor. Sci. **1**, 319 (2013).
44. M. Dutta, A. Deb, D. Das, and V. S. K. Mattaparthi, Biointerface Res. Appl. Chem. **11**, 8804 (2021).
45. M. J. S. Dewar and W. Thiel, J. Am. Chem. Soc. **99**, 4899 (1977).
46. M. J. S. Dewar, E. G. Zoebisch, E. F. Healy, and J. J. P. Stewart, J. Am. Chem. Soc. **107**, 3902 (1985).
47. *HyperChem 7.0* (Hypecube Inc., Gainesville, FL, USA, 2001).
48. L. T. Cai, J. L. Bahr, Y. X. Yao, and J. M. Tour, Chem. Mater. **14**, 4235 (2002).
49. S. Banerjee and S. S. Wong, J. Phys. Chem. B **106**, 12144 (2002).